

Assessing Characteristic Rotation Measure Values in Galactic Plasma Nebulae

Shelby Laychak

Thesis Advisor: Allison H. Costa

May 2020

Department of Astronomy

University of Virginia

This thesis is submitted in partial completion of the requirements of the BA Astronomy Major

## 1. Abstract

Supernova remnants (SNRs) and HII regions are plasma structures, which means that their magnetic fields should be important to asset their dynamic and evolutionary processes. In this paper, the populations of the characteristic rotation measure ( $RM_{char}$ ) values between HII regions and supernova remnants were explored. They were tested to see if they are significantly similar at a p-value of 0.05. The null hypothesis is  $H_0: \mu_1 = \mu_2$ , while the alternative hypothesis is  $H_a: \mu_1 \neq \mu_2$ . First, catalogs of the HII regions and SNRs were matched with the RM value catalogs. Then, a version of a one-way ANOVA test for two populations was conducted. Populations at  $d < r_{neb}$  compared with  $r_{neb} < d < 2r_{neb}$  of HII regions were tested to be significantly similar populations with a p-value of 0.668. Populations at  $d < r_{neb}$  compared with  $r_{neb} < d < 2r_{neb}$  of SNRs were tested to be significantly similar populations with a p-value of 0.586. At  $d < r_{neb}$  of HII regions compared with  $d < r_{neb}$  of SNRs, were tested to be significantly similar populations with a p-value of 0.124. As for populations at  $r_{neb} < d < 2r_{neb}$  of HII regions compared with  $r_{neb} < d < 2r_{neb}$  of SNRs, were tested to be significantly similar populations with a p-value of 0.916. Therefore, I failed to reject the null hypothesis.

## 2. Introduction

O and B stars dramatically alter their natal molecular environments throughout their lives. When on the Main Sequence, these massive stars will photoionize the surrounding gas, creating plasma structures called HII regions. The extent of an HII region is characterize by the balance between the rate of ionization and the rate of recombination of hydrogen, as conically described by the Strömgren sphere. Typically, HII regions are described by a low density cavity surrounded by a thin plasma shell (Chapter 11 of Draine 2011).

Main sequence stars also have energetic stellar winds, which can sweep up surrounding material to inflate a bubble structure around the stars. In the Weaver et al. 1977 solution for a wind blown bubble, the terminal wind velocity,  $v_\infty$ , and mass loss rate,  $\dot{M}$ , are critical parameters to determine the properties of the bubble, e.g.,space, size, density, and shock conditions in the shell.

At the end of their lives, O and B star will supernova (SN) in a core-collapse event, which dramatically modifies the surrounding material. The initial phase of a SN has ejection velocities of  $\sim 10^4 \text{ km s}^{-1}$ , but shock velocity will decrease over time as the supernova remnant expands and cools until the shock velocity equals the sound speed of the surrounding gas (see Cioffi et al. 1988 for a review). At that time, the remnant is thought to merge with the interstellar medium (ISM).

HII regions and SNRs are plasmas, so magnetic fields should be important to the dynamics and evolution of these structures. Magnetic fields are difficult to measure in astrophysics objects however. One radio observational technique is to measure the phenomenon of Faraday rotation, which is when the plane of polarization of a radio wave is rotated as it passes through a magnetized

plasma. The equation describing Faraday rotation is

$$\chi = \chi_0 + \left[ \left( \frac{e^3}{2\pi m_e^2 c^4} \right) \int_0^L n_e \vec{B} \cdot d\vec{s} \right] \lambda^2 \quad (1)$$

where  $\chi$  is the polarization position angle,  $\chi_0$  is the intrinsic polarization position angle,  $e$  is the fundamental electric charge,  $m_e$  is the mass of the electron,  $c$  is the speed of light,  $n_e$  is the electron density,  $\vec{B}$  is the magnetic field,  $d\vec{s}$  is the incremental pathlength interval along the line of sight, and  $\lambda$  is the wavelength. The integral in Equation (1) is taken from the source at  $s = 0$  to the observer at  $s = L$ , and therefore the variable  $L$  represents the effective thickness of the plasma. The quantity in square brackets is defined as the rotation measure (RM) and is equal to a change in polarization position angle over a change in wavelength. Rewriting Equation (1) for the RM and in an expression which gives an SI value for the RM in mixed but convenient interstellar units is

$$\text{RM} = 0.81 \int_0^L n_e (\text{cm}^{-3}) \vec{B} (\mu\text{G}) \cdot d\vec{s} (\text{pc}) \text{ rad m}^{-2} \quad (2)$$

To probe the plasma structure of HII regions and SNRs, linearly polarized radio sources with lines of sight through or near to the structure are chosen for observations. With a number of lines of sight and knowledge of the electron density of the nebula, it is possible to extract information about the line of sight component of the magnetic field ( $B_{los}$ ). A review of this observational technique is available in Savage et al. (2013).

The goal of this paper is to determine a characteristic RM value for HII regions and supernova remnants. To achieve this, I match lines of sight with associated RM values to plasma structures using data available in the literature. I define the characteristic,  $\text{RM}_{char}$ , to be the average of the absolute value of the RM value for all the lines of sight through a nebula. I also define a background RM value,  $\text{RM}_{bkg}$ , to be the average of the absolute value of the RM value associated with sources whose lines of sight that do not intersect with the plasma structure of HII regions or SNRs. This work represents a contribution towards a larger goal of understanding the magnetic field in different astrophysical plasmas like HII regions, SNRs, and planetary nebula when accounting for size, electron density, and age.

### 3. Data From Literature

I utilize catalogs available in the literature for matching lines of sight (LOS) with RM values to nebulae. The Xu and Han (Xu J. Han J.L. 2014), and the Taylor et. al 2009 catalogs of RM values is used along with the WISE HII regions catalog (Anderson et al., 2014). The RM catalogs are also used along with the MOST (Whiteoak et al. 1996) and Green (Green, D. A. 2017) catalogs of SNR measurements. The Xu and Han catalog is a collection of RM values from the literature from 99 papers <sup>1</sup>

---

<sup>1</sup>A full list of the papers is available at <http://zmtt.bao.ac.cn/RM/DataRef.html>

The Xu and Han catalog contains 5266 sources with associated RM values published in the literature. In addition to the Xu and Han catalog, I utilize the Taylor et al. (2009) catalog of 37543 RM values, which was created using the NVSS polarimetric data. These sources are typically extra galactic radio sources, and the RM values are determined from measurements of the polarization position angle at two or more wavelengths. Figure 1 is a Mollweide plot in galactic coordinates ( $\ell$  and  $b$ ) showing the sources from the RM values catalog. The size of the dots are scaled to the absolute value of the RM measurements. The red circles represent negative RM values and the blue ones are positive RM values. The color of the symbols represents the sign of the RM value, which gives the sign of  $B_{los}$ . Given the convention in Equation (1), a positive value of the RM indicates a line of sight component of the magnetic field directed towards the observer and away from an observer for a negative value of the RM.

Figure 2 is a Mollweide plot in  $\ell$  and  $b$  of the RM measurements from the Taylor et al. (2009) catalog. The blue values represent positive RM measurements while the red values represent negative RM measurements.

The Green catalog of SNRs has 295 entries. The catalog contains the galactic coordinates and radii of the SNRs. The MOST catalog also gives the galactic coordinates and radii of 93 SNRs. Figure 3 shows the distribution of the SNRs in the plane of the sky. The Green catalog is represented by the green filled circles, while the MOST catalog is represented by the black filled circles. The size of the filled circles is scaled to the log of the radius. There are no SNRs in the MOST and Green catalogs outside of  $-30^\circ < b < 30^\circ$ .

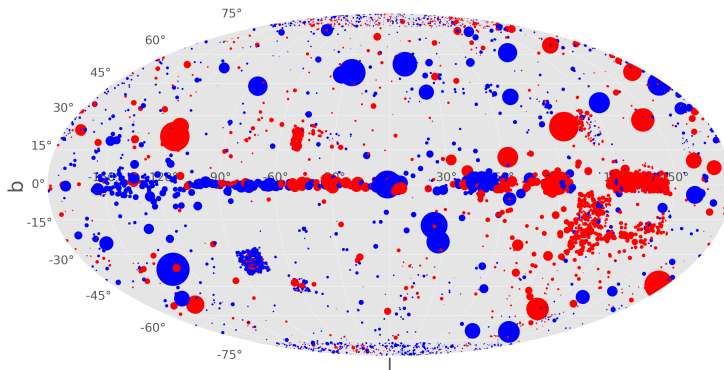


**Fig. 1.**—A Mollweide plot in galactic latitude ( $b$ ) vs. galactic longitude ( $\ell$ ) of the RM values showing the sources from the Xu and Han (Xu J. Han J.L. 2014) RM values catalog. The blue values represent positive RM values while the red values represent negative RM values. The size of the filled circles is scaled to the absolute value of the RM measurement.

The WISE catalog of HII regions has 8407 entries (Anderson et al. 2014). Each entry lists the coordinates and the angular radius of the HII region. Figure 4 is similar to Figure 3 but shows the

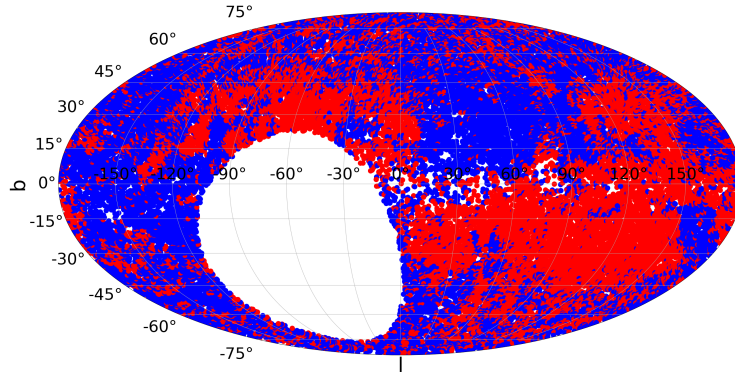


**Fig. 2.**—A Mollweide plot in  $b$  vs.  $l$  of the RM values showing the sources from the Taylor et al. (2009) RM values catalog. The blue values represent positive RM values while the red values represent negative RM values.

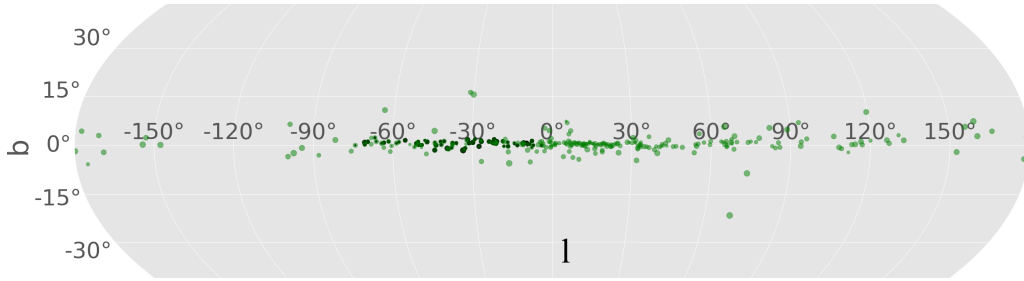


**Fig. 3.**—A Mollweide graph of SNRs  $b$  vs.  $l$  from the Green (Green, D. A. 2017) and MOST (Whiteoak et al. 1996) catalogs. The Green catalog is represented by the green filled circles while, the MOST catalog is represented by the black filled circles. The size of the filled circles is scaled to the log of the radius. There are no SNRs in the MOST and Green catalogs outside of  $-30^\circ < b < 30^\circ$ .

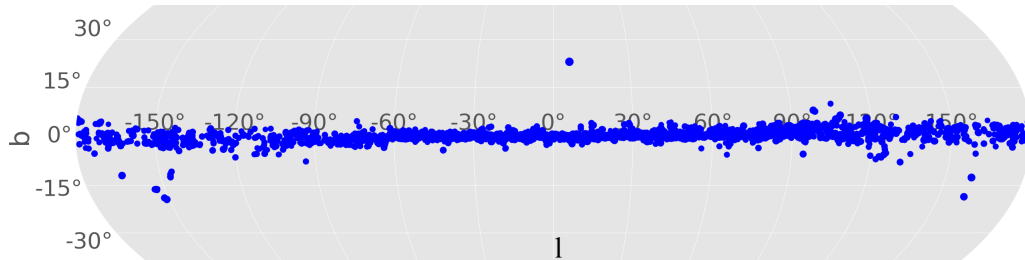


**Fig. 4.**—A Mollweide plot in  $b$  vs.  $l$  of HII regions from the WISE (Anderson et al., 2014) catalog. The size of the filled circles is scaled to the log of the radius. There are no HII regions in the WISE catalog outside of  $-30^\circ < b < 30^\circ$ .

locations of the HII regions from the WISE catalog. The size of the dots are scaled to the log of the HII region’s radius. This figure shows the distribution of HII regions. As seen in the plot, the HII regions are in the galactic plane.

## 4. Data Analysis

### 4.1. Matching Lines of Sight with RM Values to Nebulae

To determine a characteristic RM for the nebulae, I match RM values with the HII regions catalog. This is completed at different angular separations from the radius of the nebula,  $r_{neb}$ . I select lines of sight with RM values that intersect the plasma shell of the nebula ( $d < r_{neb}$ ). To determine the characteristic background RM measurement, I also select LOS that are nearby but exterior to the plasma shell ( $r_{neb} < d < 2r_{neb}$ ). To an observer,  $d$  represents the angular separation of the plane of the sky from the center of the nebula to the line of sight.

After matching the RM value catalog with the HII region catalog, the average absolute value of the RM values,  $RM_{char}$ , is calculated. This is done at each angular separation from the radius of the HII regions. These histograms (Figures 4-6) show the distribution of the RM values at each distance. Then, the SNR catalogs are matched with the RM value Taylor et al. and Xu and Han catalogs. This is done for LOS within the SNR ( $d < r_{neb}$ ), and for LOS between  $r_{neb} < d < 2r_{neb}$  of the SNR.

To match RM values with HII Regions or SNRs data, I did this by writing a program in Python. Two empty dictionaries are created one for RM values and another for nebulae values. Then there are a series of conditional statements saying that if the lines of sight with RM values longitude is less than the center coordinate of the nebula +  $r_{neb} \times$  tolerance, then it is added to the empty RM values dictionary. The tolerance parameter is a scalar to probe different distances from the center of the nebula. For galactic latitude, if the galactic latitude of the RM values is less than the nebulae latitude +  $r_{neb} \times$  tolerance, then add it to the empty RM values dictionary. I treat each size of the nebula as spherical because not all entries in the catalogs have a semi-major or a semi-minor axis recorded. With this, the code then finds where the logical AND of these two statements are true to match the line of sight with the nebula. The output of the matching code is a database of nebula matched with lines sight with RM values. In this output, it includes the nebula index, its galactic coordinates, radius and radius error. Along with the nebula data, there are the LOS with RM values, the RM values’ galactic coordinates, and the error associated with the RM values. The database is then stored as a json file.

### 4.2. Average Values of $|RM|$

The procedure is as follows

- Identifies lines of sight with associated RM values whose angular separation from the center of the nebula,  $d$ , is less than the radius of the nebula,  $r_{neb}$  for each entry in the HII region and SNR catalogs.
- Determined the average of the absolute value of the RM values associated with each nebula. This is the  $RM_{char}$  for that particular nebula.
- Created histograms of the  $RM_{char}$  of each nebula and a histogram of the number of total sources with RM values per each nebula.
- Created histograms for the radius for the entire WISE, Green, and MOST catalogs. Then, I made histograms for the radius of the matched sample found,  $RM_{char}$ , for HII regions and SNRs
- Calculated weighted average, median, and mode for the sample and entire catalog size histogram.
- Plotted the size of the nebula vs.  $RM_{char}$  for the sample of nebulae with associated RM values. Calculated the weighted mean, median, and mode for the averaged  $|RM|$  per nebula.

### 4.3. ANOVA Testing

One-way Analysis of Variance (ANOVA) testing is selected to test the significance between nebulae. ANOVA testing is used for testing 2+ populations. I retain the framework of an ANOVA testing for future applications, which will expand the population testing to include a third population. By significance, I am asking if the means of the populations are different? It is used to test between groups and here the groups are the HII regions and SNRs. The purpose is to test for differences in the average of the dependent variable (RM values) of the independent variable (nebulae) (IDRE Stats).

For this paper, testing was done between similar radii in the different nebulae and different radii in the same nebulae e.g.,  $d < r_{HII}$  and  $d < r_{SNR}$ . This is to determine if the characteristic RM values between the two different nebulae are statistically different. The null hypothesis is  $H_0: \mu_1 = \mu_2$ , where  $\mu$  are the  $RM_{char}$  values. The alternative hypothesis is  $H_a: \mu_1 \neq \mu_2$ .

## 5. Results

### 5.1. Graphs and Tables

In total there were 108 HII regions and 91 SNRs that have matched the lines of sight with the RM values for  $d < r_{neb}$ . Table 1 lists the average  $RM_{char}$ ,  $267 \text{ rad m}^{-2}$  for all HII regions

and 307 rad m<sup>-2</sup> for all SNRs. The range for this  $RM_{char}$  is 1-876 rad m<sup>-2</sup> for HII regions and 1.90-1.34×10<sup>3</sup> rad m<sup>-2</sup> for SNRs.

In Table 1, there is also a section for  $r_{neb} < d < 2r_{neb}$ . The number of nebula with one or more LOS is 91 for HII regions and 88 for SNRs. The average  $RM_{bkg}$  is 272 rad m<sup>-2</sup> for HII regions and 279 rad m<sup>-2</sup> for SNRs. While the range for  $RM_{bkg}$  is 0-4.77×10<sup>3</sup> rad m<sup>-2</sup> for HII regions and 0-2.84×10<sup>3</sup> rad m<sup>-2</sup> for SNRS.

For $d < r_{neb}$	HII Regions	SNRs
Number of Nebula with one or more LOS	108	91.0
$ RM_{char} $ (rad m <sup>-2</sup> )	267	307
Range of $ RM_{char} $ (rad m <sup>-2</sup> )	1-876	1.90-1.34×10 <sup>3</sup>
For $r_{neb} < d < 2r_{neb}$	HII Regions	SNRs
Number of Nebula with one or more LOS	91.0	88.0
$RM_{bkg}$ (rad m <sup>-2</sup> )	272	279
Range of $RM_{bkg}$ (rad m <sup>-2</sup> )	0-4.77×10 <sup>3</sup>	0-2.84×10 <sup>3</sup>

**Table 1:**

In Table 2, it shows the values that I calculated for the weighted mean, average median, and average mode for the  $RM_{char}$ . The weighted mean is described as the total of the sum of the RM values divided by the number of elements of RM values. The average median is the middle value when the list of values is sorted. The average mode is described as the value that appears the maximum number of times. For HII regions, the weighted mean is 258 rad m<sup>-2</sup>, the average median value is 134 rad m<sup>-2</sup>, and the average mode value is 11.1 rad m<sup>-2</sup>. For SNRs, the weighted mean is 293 rad m<sup>-2</sup>, the average median value is 167 rad m<sup>-2</sup>, and the average mode value is 110 rad m<sup>-2</sup>.

Averaged $ RM $ Per Nebula	HII Regions	SNRs
Weighted Mean	258rad m <sup>-2</sup>	293rad m <sup>-2</sup>
Average Median Value	134rad m <sup>-2</sup>	167rad m <sup>-2</sup>
Average Mode Value	11.1rad m <sup>-2</sup>	110rad m <sup>-2</sup>

**Table 2::** *Weighted Mean, Average Median, and Average Mode of all the RM values associated with a nebula.*

Figures 5 and 6 show the  $RM_{char}$  values at each radii for HII regions. Figure 5 shows a peak at 100 rad m<sup>-2</sup> with 14 counts. There is another peak from 0-25 rad m<sup>-2</sup> with 13 counts. While for Figure 6, there is a peak at 100 rad m<sup>2</sup> with 10 counts.

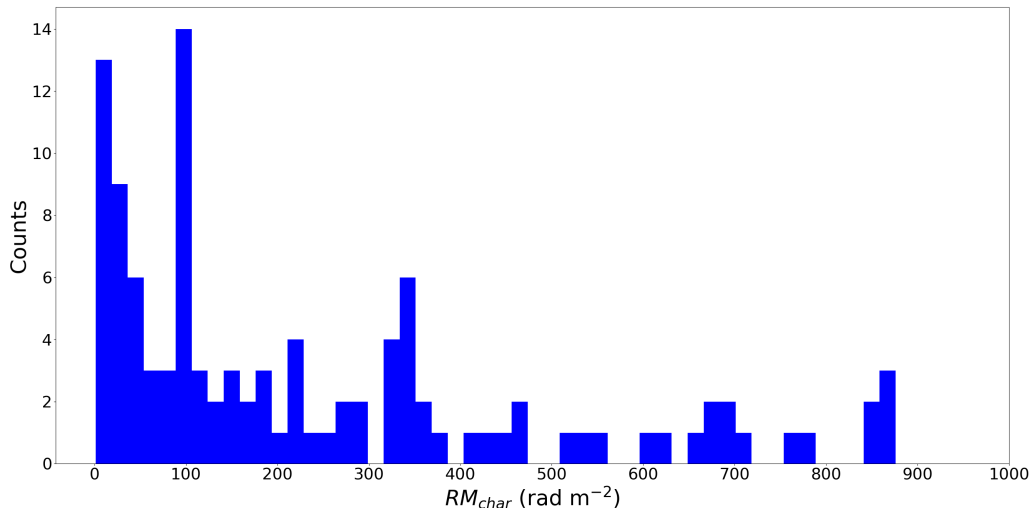
Figures 7 and 8, show the  $RM_{char}$  values at each radii for SNRs. For Figure 7, most of the data falls on the left hand side below 300 rad m<sup>-2</sup> with a peak around 100 rad m<sup>2</sup> with 10 counts. Figure 8 shows the average RM values from  $r_{neb} < d < 2r_{neb}$ . There is also a peak a little less than



100 rad m<sup>-2</sup> with 10 counts. When compared to Figures 5 and 6, all figures have data that mainly falls on the left hand side and have peaks around 100 rad m<sup>-2</sup>. Most of the RM values matched to HII regions and SNR are small in magnitude, which means that for most of these nebula, there is not an enhanced RM signature in these plasma structures.

Figures 9 and 10 show the number of LOS through the HII regions. In Figure 9, 80 out of the 108 HII regions in the sample have 1 LOS through them, but there is one HII region that has 80 LOS through it. While in Figure 10, there are around 60 nebulae with 1 LOS, and 1 nebula with around 90 and 110 LOS. The nebula that have many LOS through them also have the largest angular radii, so it is not surprising that they have the most LOS.

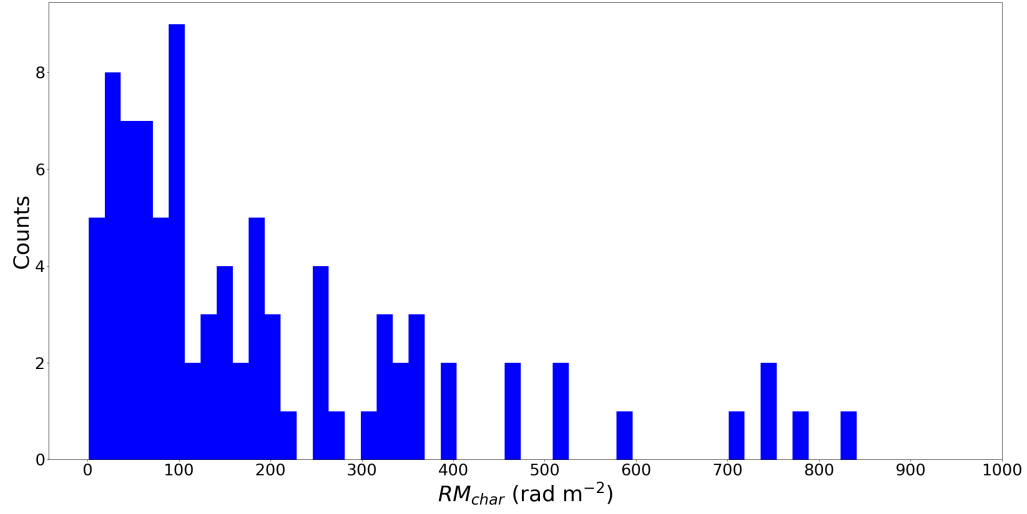
Figures 11 and 12 show the number of LOS through the SNRs. Figure 11 shows a peak at 1 with around 60 nebulae having 1 LOS through a SNR. The most LOS a SNR has is around ~ 110, and that SNR has an angular radius of 5.5°. Figure 12 shows a peak at 1 with around 60 nebulae having 1 LOS. The most LOS through a SNR between  $r_{neb} < d < 2r_{neb}$  has is 137 and it is again, the SNR with a radius of 5.5°.



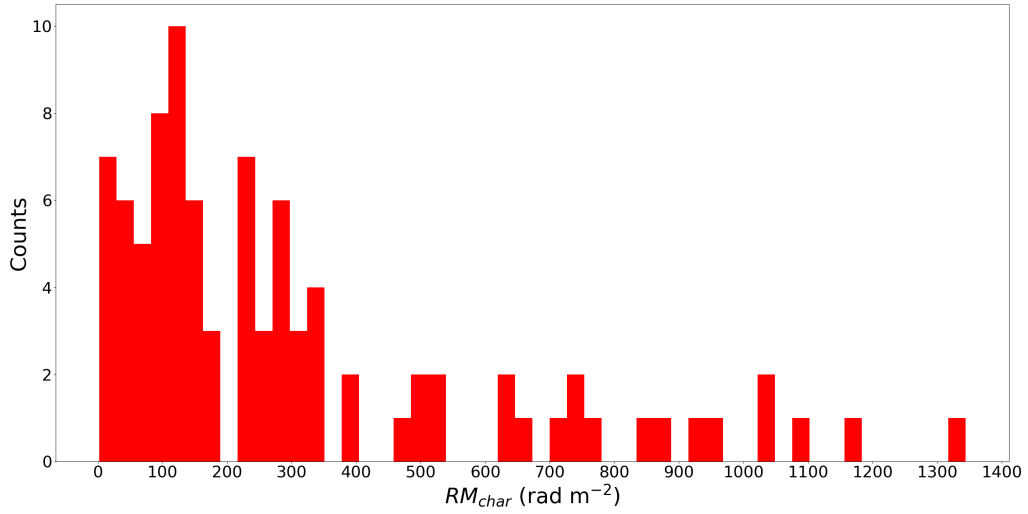
**Fig. 5.**—Histogram of  $RM_{char}$  at  $d < r_{neb}$  of the HII region.

Figure 13 is a histogram of the radii of the entire WISE HII region catalog, while Figure 14 shows the radii for the sample of HII region matched with LOS for this study. From these graphs, it is seen that there are more bigger radii in the sample than in the catalog. This is because a bigger radii is going to be easier to see than a smaller radii, therefore, making it easier to match RM values.

Figure 15 shows the radius of the catalog of SNRs while Figure 16 shows the sample I collected of matching SNRs. Similarly the HII regions, there are more larger radii of SNRs than smaller in



**Fig. 6.**—Histogram of the  $RM_{char}$  at  $r_{neb} < d < 2r_{neb}$  from the center of the HII region.



**Fig. 7.**—Histogram of the  $RM_{char}$  at  $d < r_{neb}$  of the HII region.

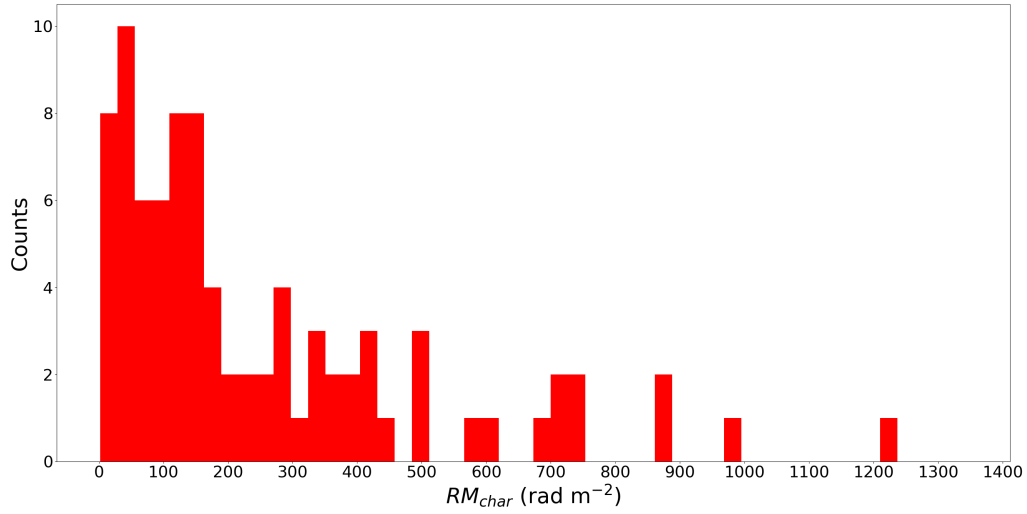


**Fig. 8.**—Histogram of the  $RM_{char}$  at  $r_{neb} < d < 2r_{neb}$  from the center of the SNR.

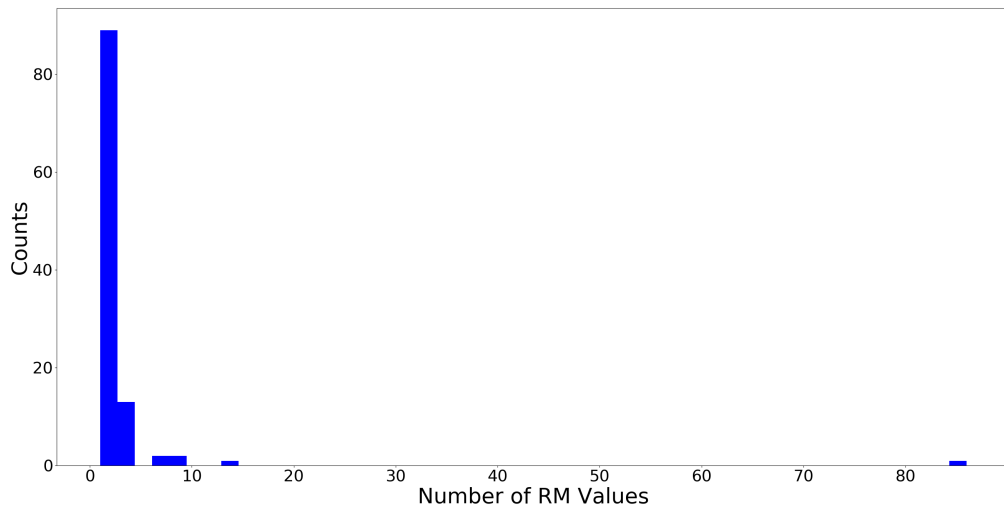


**Fig. 9.**—Histogram of the number LOS inside the HII region at  $d < r_{neb}$ .

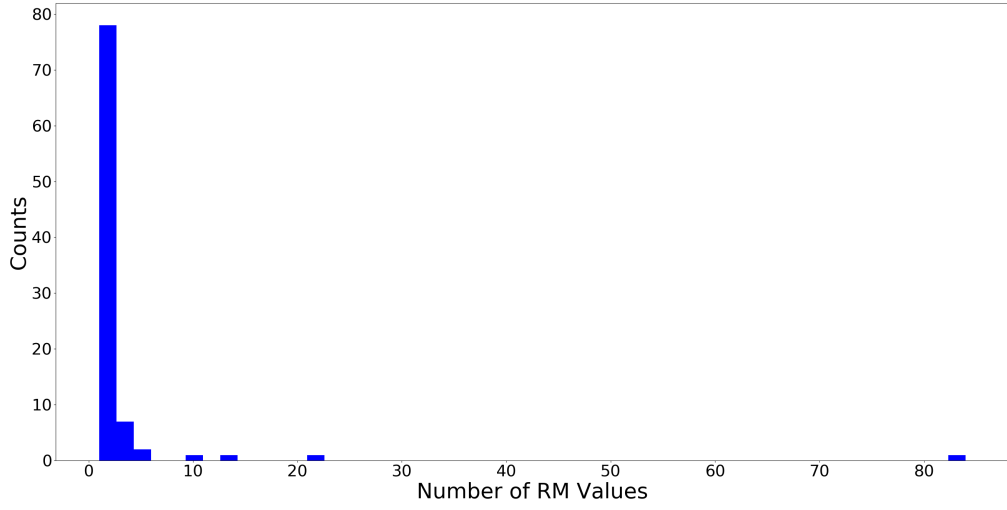


**Fig. 10.**—Histogram of the number of LOS per nebula at  $r_{neb} < d < 2r_{neb}$  from the center of the HII region.

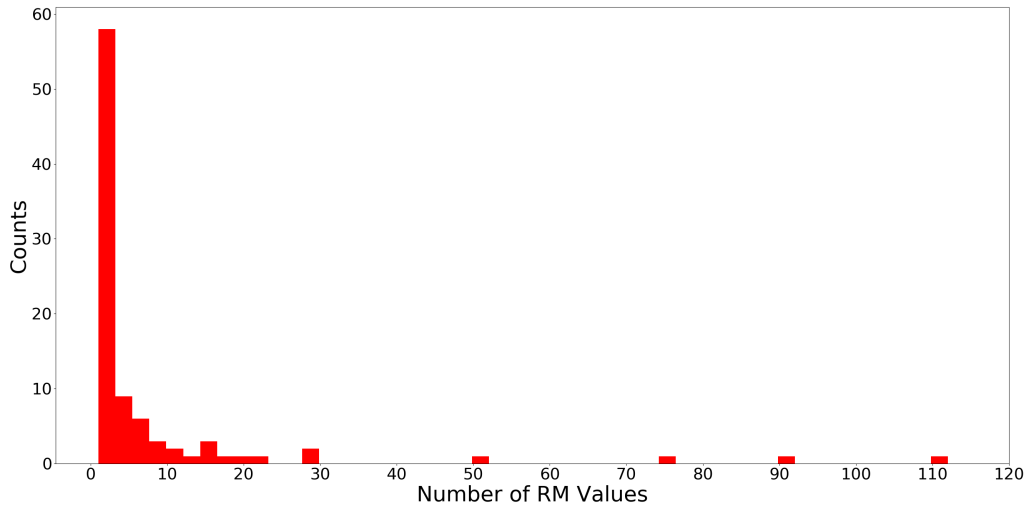


**Fig. 11.**—Histogram of the number LOS inside the SNR at  $d < r_{neb}$ .

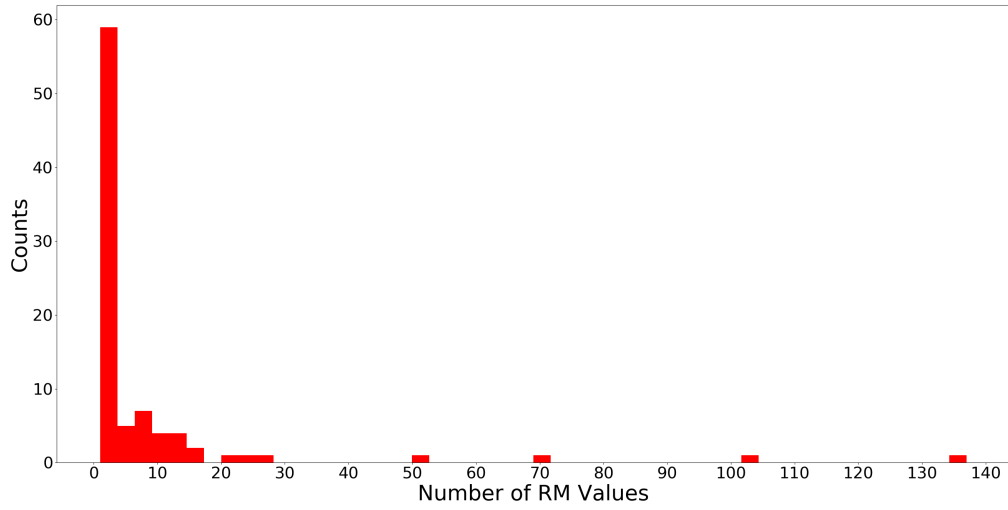


**Fig. 12.**—Histogram of the number LOS per nebula at  $r_{neb} < d < 2r_{neb}$  from the center of the SNR.

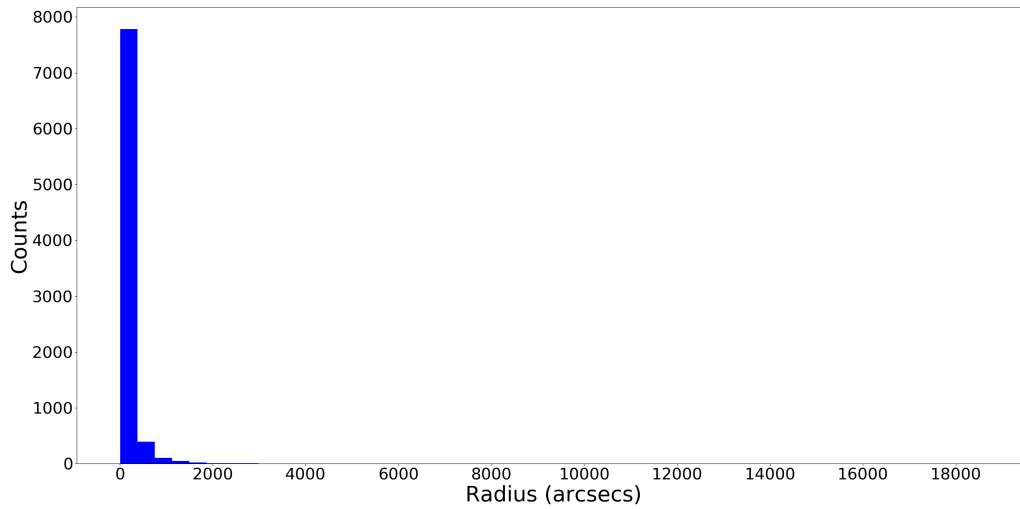


**Fig. 13.**—Histogram of all HII sources from the WISE catalog.

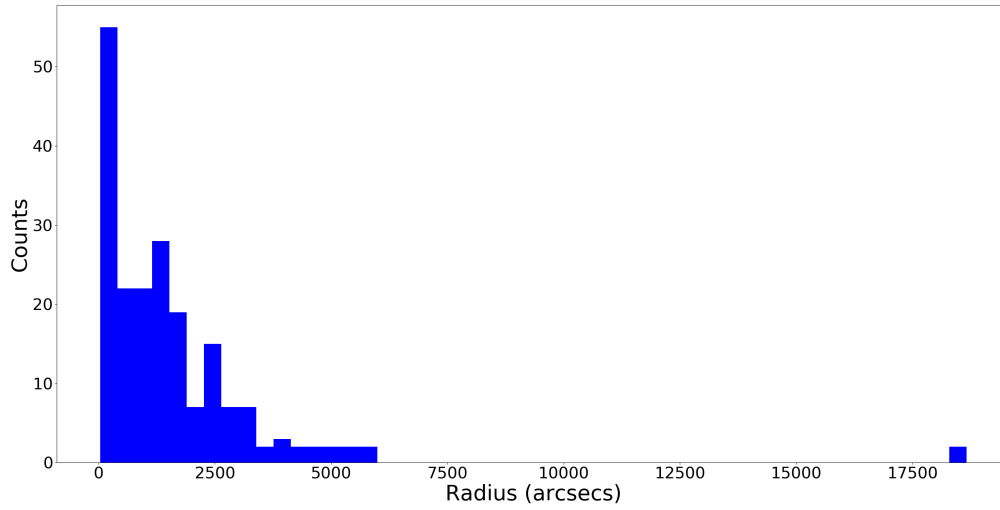


**Fig. 14.**—Histogram of the matched HII regions from the WISE catalog with the RM values from the Xu and Han, and Taylor et al. (2009) catalogs.

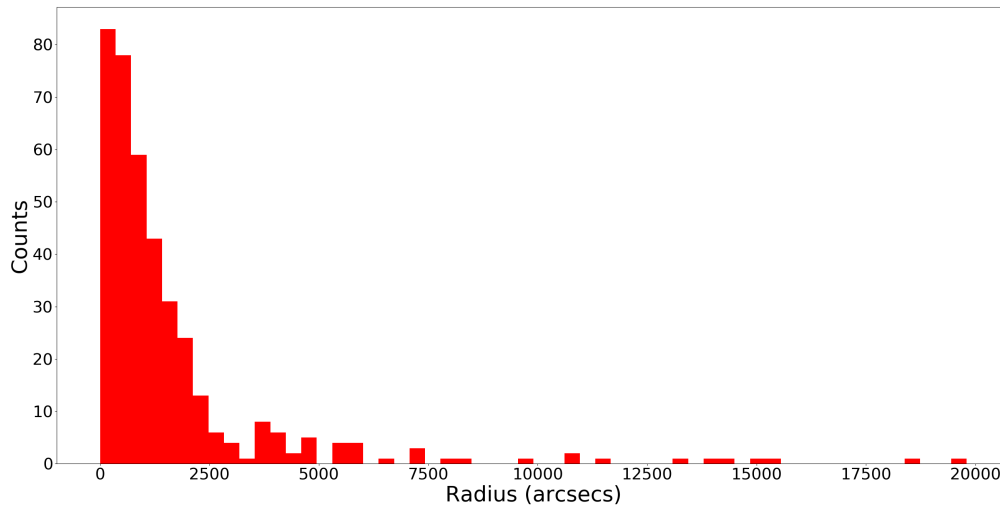


**Fig. 15.**—Histogram of all SNR sources from the MOST and Green catalogs.

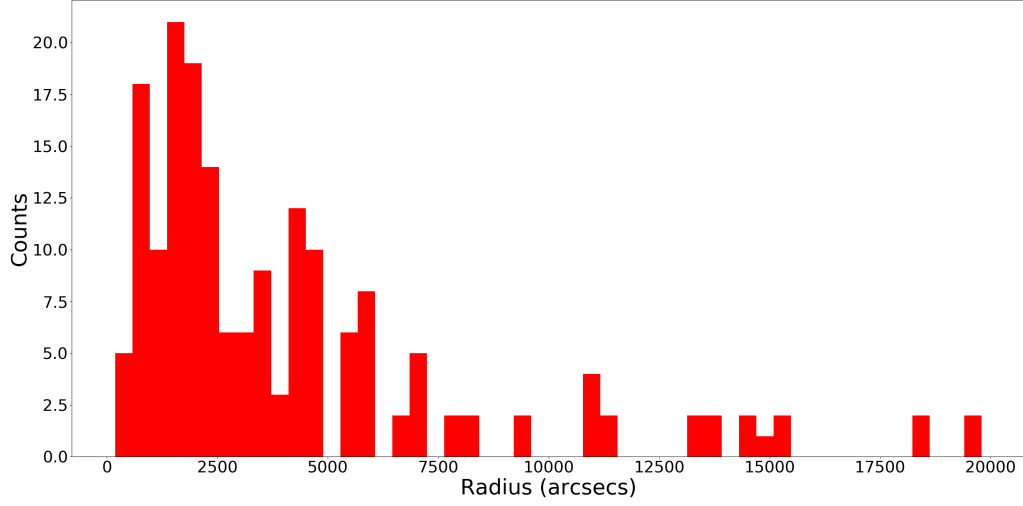


**Fig. 16.**—Histogram of the matched SNR sources from the MOST and Green catalogs with the RM values from the Xu and Han, and Taylor et al. (2009) catalogs.

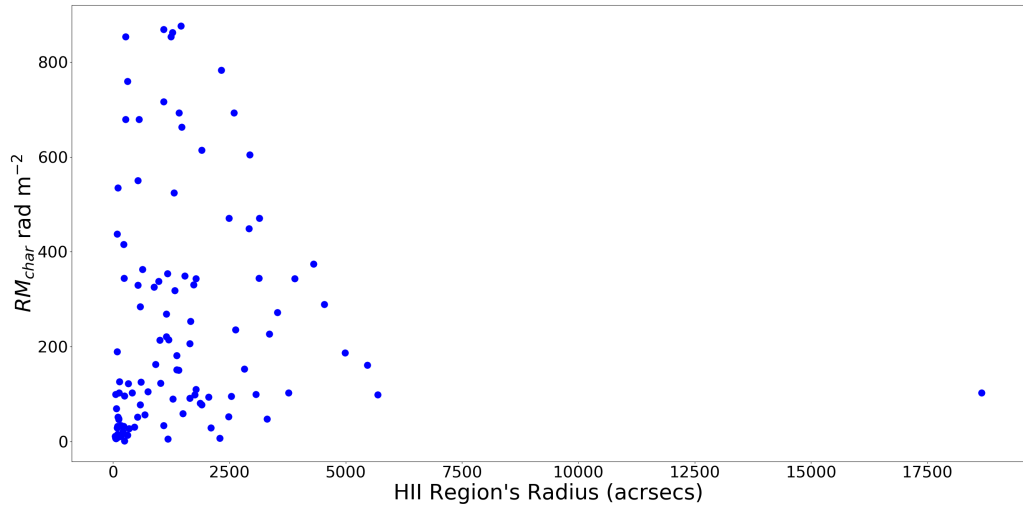


**Fig. 17.**—A scatterplot of the radius in arcsecs of HII regions vs.  $RM_{char}$  in  $\text{rad m}^{-2}$ . This is done at  $d < r_{neb}$ .

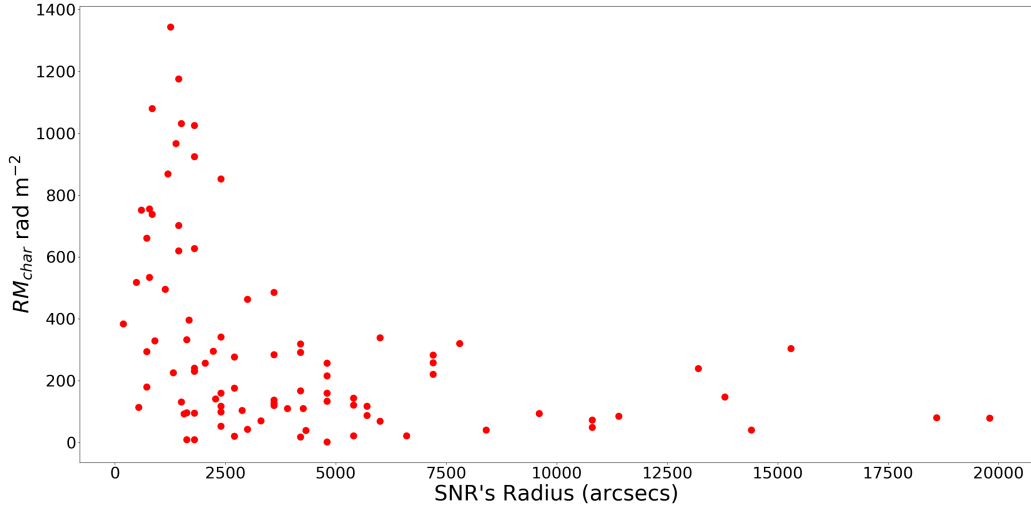


**Fig. 18.**—A scatterplot of the radius in arcsecs of SNRs vs.  $RM_{char}$  in  $\text{rad m}^{-2}$ . This is done at  $d < r_{neb}$ .

the sample size.

Figures 17 and 18 are scatterplots of the nebula’s radius vs the  $RM_{char}$  value at  $d < r_{neb}$ . Figure 17 shows that most HII regions are between 0 and 5000 arcsecs with a  $RM_{char}$  less than 800  $\text{rad m}^{-2}$ . In Figure 18, there are more circle variation than the HII region’s scatterplot. The circles along the  $RM_{char}$  value axis double than what is seen in Figure 17. Most SNRs are between 0 and 20000 arcsecs with  $RM_{char}$  less than 1400  $\text{rad m}^{-2}$ .

After graphing, I conduct an ANOVA test on different regions to test against the null hypothesis which is  $\mu_1 = \mu_2$ . Table 3 lays out the different p-values and sample sizes. If the p-value is higher than 0.05, then the null hypothesis is not rejected with significance. If the null is not rejected, then the differences in the mean between the populations can be explained by chance. The test shows that different nebulae compared at similar radii are significantly similar populations. The p-values for this test were 0.668 for HII regions and 0.586 for SNRs with sample sizes of 199 and 179. HII regions of  $d < r_{neb}$  compared with  $d < r_{neb}$  of SNRs are tested to be significantly similar populations with a p-value of 0.124 and sample size of 199. Between  $r_{neb} < d < 2r_{neb}$  away from the nebulae are significantly similar populations as well with a p-value of less than 0.916 and a sample size of 179.



HII Regions	p-values	Sample Size
$r_{neb}$ and $r_{neb} < d < 2r_{neb}$	0.668	199
SNRS	p-values	Sample Size
$r_{neb}$ and $r_{neb} < d < 2r_{neb}$	0.586	179
HII and SNRS	p-values	Sample Size
$r_{neb}$	0.124	199
$r_{neb} < d < 2r_{neb}$	0.916	179

**Table 3::** *p-values*

## 6. Conclusion

With this work, I have identified a sample of nebula with LOS with RM values. From the ANOVA test, I conclude that there is not a significant difference in the characteristic RM value between HII regions and SNRs, despite them being vastly different astronomical objects. With this sample, a future project would include collecting information about electron density for these nebulae and determining if the LOS passes through the the cavity of the nebula or through the shell, which may have shocks and thus may have a larger character RM value (Savage et al. 2013). With this additional information, I can revisit these results of this study.

To summarize this study, first, catalogs of the HII regions and SNRs were matched with the RM value catalogs. A one-way ANOVA test for two populations was conducted. The null hypothesis is  $H_0: \mu_1 = \mu_2$ , and the alternative hypothesis is  $H_a: \mu_1 \neq \mu_2$ . The two populations are the average RM values of the HII regions and SNRs. Populations at  $d < r_{neb}$  compared with  $r_{neb} < d < 2r_{neb}$  of HII regions are tested to be significantly similar populations. Similarly populations at  $d < r_{neb}$  compared with  $r_{neb} < d < 2r_{neb}$  of SNRs are tested to be significantly similar populations. Then, populations at  $d < r_{neb}$  of HII regions compared with  $d < r_{neb}$  of SNRs, they are significantly similar populations. As for populations at  $r_{neb} < d < 2r_{neb}$  of HII regions compared with  $r_{neb} < d < 2r_{neb}$  of SNRs are tested to be significantly similar populations. Due to all of these test having a p-value greater than 0.05, I fail to reject the null hypothesis.

### 6.1. Future Work and Improvements

For future works, I want to compare to more than two different types of nebulae such as adding in data of protoplanetary nebulae. After that, an ANOVA test can be conducted for the three different nebulae populations. I could also add in another population of HII regions that include Ultra Compact HII regions. However, this study is ultimately limited to the number of LOS through a nebula, and the smaller nebula will naturally have few LOS through them compared to larger nebula. To improve this paper, the results would be more accurate if it was not assumed that the objects being studied are spherical. By relaxing this assumption, I can better account for

the individual morphology of the nebulae. Out of over 5,000 values in the HII regions catalog, less than 200 values were found. For the SNR catalog, only 179 values were found out of close to 400. Another limitation that goes along with the spherical assumption, was that I was limited by the amount of data available.

## REFERENCES

- Anderson, L.D., Bania, T.M., Balser, D.S., Cunningham, V., Wenger, T.V., Johnstone, B.M., and Armen trout, W.P. 2014, ApJ
- ”WHAT STATISTICAL ANALYSIS SHOULD I USE? STATISTICAL ANALYSES USING SPSS”  
IDRE Stats. UCLA.
- Cioffi, D. F., McKee, C. F., & Bertschinger, E. 1988, ApJ, 334, 252
- Draine, B. T. 2011, Physics of the Interstellar and Intergalactic Medium by Bruce T. Draine.  
Princeton University Press
- Green, D. A. 2017, Vizier Online Data Catalog
- Savage A. H., Spangler S. R. and Fischer P. D. 2013 ApJ, v.765, no.1
- Taylor, A.R, Stil, J.M., and Sunstrum, C. 2009, ApJ, 702, 1230.
- Weaver, R., McCray, R., Castor, J., Shapiro, P., and Moore, R. 1977 ApJ, vol. 218, no.1, p.377-395.
- Whiteoak, J. B. Z., Green, A. J. 1996, Astronomy and Astrophysics supplement, , v.118, p.329-380
- Xu, J., Han, J. L. 2014, RAA, Vol.14, p. 942-958.